Published in final edited form as:

Curr Biol. 2019 February 18; 29(4): 592–604.e4. doi:10.1016/j.cub.2019.01.022.

Kisspeptin Neurons in the Arcuate Nucleus of the Hypothalamus Orchestrate Circadian Rhythms and Metabolism

Stephanie L. Padilla[1,2,5,*], **Jazmine G. Perez**[3], **Miriam Ben-Hamo**[3], **Christopher W. Johnson**[4], **Raymond Sanchez**[3,4], **Ivana Bussi**[3], **Richard D. Palmiter**[1,‡], **Horacio O. de la Iglesia**[3,‡,*]

[1]Howard Hughes Medical Institute, University of Washington, Seattle, WA 98195, USA.

[2]Present address: Department of Biology, University of Massachusetts, Amherst, MA 01003, USA.

[3]Department of Biology, University of Washington, Seattle, WA 98195, USA.

[4]Graduate Program in Neuroscience, University of Washington, Seattle WA 98195, USA.

[5]Lead contact

SUMMARY

Successful reproduction in female mammals is precisely timed and must be able to withstand the metabolic demand of pregnancy and lactation. We show that kisspeptin-expressing neurons in the arcuate hypothalamus (Kiss1^{ARH}) of female mice control the daily timing of food intake along with the circadian regulation of locomotor activity, sleep and core body temperature. Toxin-induced silencing of Kiss1^{ARH} neurons shifts wakefulness and food consumption to the light phase and induces weight gain. Toxin-silenced mice are less physically active and have attenuated temperature rhythms. Because the rhythm of the master clock in the suprachiasmatic nucleus (SCN) appears to be intact, we hypothesize that Kiss1^{ARH} neurons signal to neurons downstream of the master clock to modulate the output of the SCN. We conclude that, in addition to their well-established role in regulating fertility, Kiss1^{ARH} neurons are a critical component of the hypothalamic circadian oscillator network that times overt rhythms of physiology and behavior.

eTOC Blurb (In Brief)

[*]To whom correspondence should be addressed, Stephanie L. Padilla (slpadilla@umass.edu), Horacio O. de la Iglesia (horaciod@uw.edu).

AUTHOR CONTRIBUTIONS

S.L.P designed the study under the guidance of H.O.D and R.D.P. Experiments were performed by S.L.P., J.G.P. and C.W.J. Data were analyzed by S.L.P, R.S, I.B and H.O.D. The script for sleep scoring and survival curves was written by M.BH. The resources and space to perform the experiments were provided by R.D. P and H.O.D. The manuscript was written by S.L.P, R.D.P and H.O.D with input from all of the authors.

[‡]Authors contributed equally to this manuscript

DECLARATION OF INTERESTS

The authors declare no competing interests.

Sex hormones can impact circadian rhythms, but the neural mechanism/s remains largely unresolved. Padilla et al. demonstrate that sex-hormone-sensitive Kiss1 neurons in the arcuate hypothalamus are a necessary component of circadian rhythms.

INTRODUCTION

In animals, activity is typically segregated into sleep:wake phases that occur on a 24-h cycle. Nocturnal species such as mice are awake and active during the night and if food is available *ad libitum* they consume most of their calories during the dark (D). Food consumption outside of this time window correlates with higher body weight [1]. Mice on a high-fat diet are protected from weight gain if feeding is restricted to the D phase, but become obese if it is consumed during the light (L) phase, despite matched caloric intake [2, 3]. Eating out-of-phase with the natural sleep:wake cycle causes metabolic disruptions in both mice and humans alike. For example, people that work night-shifted hours are awake and eat during the body's natural sleep phase and have a higher incidence of metabolic disruptions, including increased body weight [4]. Together, these findings underscore the importance of circadian timing of food consumption as a critical variable that influences body weight homeostasis and suggest interventions to promote weight loss [5].

In mammals, the biological time-keeping system is orchestrated by master-oscillator cells in the suprachiasmatic nucleus (SCN) of the hypothalamus [6]. These synchronized circadian oscillators are driven by transcriptional-translational feedback loops involving a set of clock genes [7]. SCN cells receive retinal input, which aligns the master clock with the environmental light:dark (L:D) cycle [8], and the output of the SCN neurons sets the rhythm of oscillators in cells throughout the brain and the rest of the body. The SCN sets the phase of peripheral oscillators in the liver [9] to regulate the expression of hundreds of genes that control metabolic programs, which prioritize catabolic (energy consuming) metabolism during the wake state, versus anabolic (energy storing) metabolism during the sleep state [10]. The circadian profile of metabolic gene expression is abrogated in mice in which food consumption is not synchronized with the master clock, potentially contributing to weight gain [3]. The mechanism(s) by which the SCN clock entrains peripheral clocks is not well established, but it presumably involves regulation of the autonomic nervous system and hormonal signaling [11]. Either way, signaling from the SCN clock to the effector systems may be modulated by various neural and endocrine inputs to align the sleep:wake cycle with behavioral and physiological oscillations including rhythms of core body temperature (T_b), hormone levels, feeding and metabolism.

In the mammalian female, the 24-h orchestration of behavioral and physiological outputs are intertwined with the reproductive estrous cycle and oscillations in ovarian hormone levels. Fertility, pregnancy and lactation require a substantial investment of energy, and there is reciprocal exchange between neural circuits that regulate energy balance and those that coordinate reproduction to assure that females have enough energy reserves to meet the demands of reproduction. Evidence supports the idea that kisspeptin (Kiss1) signaling is central to this exchange. Kiss1 receptor knock-out mice become obese, despite consuming fewer calories than control littermates with intact Kiss1 signaling, and this phenotype is

sexually-dimorphic, occurring only in females [12]. Furthermore, in the absence of Kiss1 signaling due to conditional ablation of Kiss1-expressing cells from birth, female mice are heavier than controls [13]. There are two populations of Kiss1 neurons in the hypothalamus that play an essential role in reproduction. Kiss1 neurons in rostral periventricular area (R3PV) are positively modulated by estrogen and are believed to drive gonadotropin-releasing hormone (GnRH) neurons and subsequent release of the pre-ovulatory-surge of luteinizing hormone from the pituitary [14-16]. There are fewer of these $Kiss1^{R3PV}$ neurons in males, further supporting a female-specific role in ovulation [17]. Of note, the pre-ovulatory surge of luteinizing hormone occurs during a narrow time window prior to the active phase [18, 19], and there is evidence to support that input from the SCN to $Kiss1^{R3PV}$ neurons is responsible for mediating the time-of-day-dependent surge [20-22]. Kiss1 neurons in the arcuate nucleus of the hypothalamus (ARH), on the other hand, are negatively regulated by both estrogen and testosterone, and are believed to regulate the frequency of pulsatile activity of GnRH neurons in a sex hormone-dependent fashion [14, 23-25]. $Kiss1^{ARH}$ neurons are necessary for fertility and are conserved in both males and females [17, 26]. $Kiss1^{ARH}$ neurons project their axons to many targets other than GnRH neurons, and beyond reproduction, they are also involved in sex-hormone-mediated thermal regulation [27-29]. Because $Kiss1^{ARH}$ neurons relay information to a diverse array of downstream targets, we suspected that they may act to translate gonadal hormone status into multiple behavioral and physiological outcomes.

$Kiss1^{ARH}$ neurons have been shown to make synaptic connections with two well-characterized populations of neurons in the ARH that express agouti-related protein (AgRP) or pro-opiomelanocortin (POMC) and are known to modulate food intake and energy homeostasis, making them an attractive target to consider with respect to gonadal-hormone sensitive body weight fluctuations [30, 31]. However, there are no data showing that activity of $Kiss1^{ARH}$ neurons affects food intake or body weight. Here, we used a loss-of-function approach in female mice to chronically silence synaptic transmission from genetically defined $Kiss1^{ARH}$ neurons to ascertain whether this would affect food intake or body weight. $Kiss1^{ARH}$-silenced mice gained weight, but they did not consume more calories than lean controls. Surprisingly, $Kiss1^{ARH}$-silenced mice presented a profound shift in the phase of food intake, consuming nearly three times the amount of food as lean controls during the light phase of the circadian day, suggesting that $Kiss1^{ARH}$ neurons impact circadian function. The experiments described herein were directed towards understanding this unexpected observation.

RESULTS

$Kiss1^{ARH}$ Neurons Influence the Circadian Phase of Feeding and Body-weight Homeostasis

To investigate the role of $Kiss1^{ARH}$ neurons on long-term food intake and body-weight homeostasis, we permanently silenced them using the light chain of the tetanus toxin (TeTx) [32-36]. Genetically defined $Kiss1^{cre}$ neurons were transduced with a TeTx transgene using stereotaxic delivery of a conditional viral vector, AAV1-DIO-GFP:TeTx. Because TeTx expression does not induce apoptosis, we can visualize TeTx-expressing $Kiss1^{cre}$ neurons

with the fused GFP reporter (Figures 1A and S1A). By 4 wk after viral delivery, $Kiss1^{ARH}$-silenced mice had gained a significant amount of weight compared to controls, injected with AAV1-DIO-YFP, and compared to their starting body weight (Figure 1B). After 8 wk, $Kiss1^{ARH}$-silenced mice were ~5 g heavier than controls ($YFP_{(n = 15)}$ = 22.85 ± 0.33 g, $TeTx_{(n=12)}$ = 28.03 ± 1.49 g). The weight gain was accounted for by an increase in fat mass ($YFP_{(n = 8)}$ = 11.3 ± 0.76%, $TeTx_{(n=8)}$ = 19.7 ± 2.90%), and a modest decrease in lean mass ($YFP_{n = 8)}$ = 80.3 ± 0.81%, $TeTx_{(n=8)}$ = 72.9 ± 2.60%). These findings are consistent with the idea that $Kiss1^{ARH}$ neurons excite anorexigenic POMC neurons and inhibit orexigenic NPY/AgRP neurons [30, 31]. Over time, the loss of input from $Kiss1^{ARH}$ neurons results in an anabolic shift in metabolism.

Surprisingly, there was no change in cumulative 24-h food intake between controls and $Kiss1^{ARH}$- silenced mice; however, we observed a dramatic change in the circadian phase of feeding (Figure 1C). The $Kiss1^{ARH}$-silenced mice ate significantly less food during the D phase (nocturnal), but compensated with increased food intake during the L phase (diurnal). For this experiment, mice were housed under a 12:12 h L:D cycle and food intake was measured in 15-min bins for 2 wk. Representative feedograms depict the distribution of food intake (Figures 1D and 1E). Mice are normally nocturnal and eat during the night. Control mice consumed ~80% of calories in the D whereas $Kiss1^{ARH}$-silenced mice consumed roughly the same amount of food during the L and D phases (Figure 1C). The diurnal shift in feeding could be a factor contributing to increased body weight because rodents gain weight if they are forced to eat out of phase with the light-entrained circadian clock or if the circadian clock is disrupted [1-3, 37-39].

We have previously shown that the conditional viral TeTx transgene is sufficient to functionally silence Cre-expressing neurons [34]. To confirm that $Kiss1^{ARH}$ neurons are functionally silent, we performed two experiments. First, we anticipated that TeTx-silenced mice would have impaired estrous cycles because $Kiss1^{ARH}$ neurons are necessary to maintain normal estrous cyclicity and fertility in female rats. YFP controls had an average cycle length of ~5 d, whereas the majority of TeTx-silenced mice were acyclic (6 of 9) or had irregular cycles (Figures 1F, 1G and S1B-D). Second, we anticipated that TeTx-silenced mice would have lower circulating levels of luteinizing hormone (LH) because $Kiss1^{ARH}$ neurons are involved in the neuroendocrine-mediated release LH. We collected 10 LH measurements over 45 min and found that the average concentration was ~40% less in TeTx-silenced females, compared to YFP controls (sampled on diestrus; Figure 1H and 1I). These data, together with histology demonstrating reporter and transcript expression patterns, are consistent with the idea that TeTx acts to functionally silence Kiss1 neurons in the ARH.

$Kiss1^{ARH}$ Signaling Promotes Locomotor Activity, Independent of Estrogen

$Kiss1^{ARH}$-silenced mice gained weight in spite of matched caloric intake, which could also be due to decreased physical activity. To track activity, we gave mice free access to a running wheel and monitored wheel activity with respect to the L:D cycle for at least 15 d. Three wk after viral transduction, $Kiss1^{ARH}$-silenced mice had ~4% of the daily wheel-activity of controls (wheel turns per 24 h; YFP = 4,242 ± 536.8 vs TeTx = 173.6 ± 68.82, $p < 0.0001$;

Figure 2A). To visualize the pattern of low-amplitude wheel activity in Kiss1^{ARH}-silenced mice, we multiplied the wheel counts per 10-min bin by a factor of 25 in the representative actograms to compare them with controls (Figure 2B). This dramatic decrease in wheel running by Kiss1^{ARH}-silenced mice is unexpected because wheel running is a naturally rewarding activity for rodents [40, 41].

Because Kiss1^{ARH}-silenced mice had reduced running-wheel activity, we sought a means to better determine their total physical activity. We tracked home-cage activity over several weeks using implanted telemetry transponders. With continuous recording, it was evident that the home-cage activity phenotype of Kiss1^{ARH}-silenced mice developed on a spectrum with respect to time following the viral injection. For ~2 wk shortly after viral injection (Figure 2C, segment 2) activity patterns were severely disrupted compared to baseline (Figure 2C, segment 1). Following this transition, activity patterns stabilized and remained relatively constant (Figure 2C, segment 3). Total locomotor activity after Kiss1^{ARH} silencing was reduced; mice were 50% less active than before viral transduction (n = 6, segment 1 = 36.05 ± 4.07 vs segment 3 = 16.66 ± 0.82, counts per 24 h x 10^{-3}; p = 0.003) and this was attributed exclusively to decreased D-phase activity by the Kiss1^{ARH}-silenced mice (Figure 2D). Despite the lower D-phase activity, the rest-activity cycle of the TeTx-silenced mice was synchronized to the 24-h L:D cycle (n = 6, period = 1436 ± 2.39 min).The decrease in overall physical activity likely contributes to the loss of lean mass and increase in body fat.

Locomotor activity may be synchronized to the L:D cycle due to the masking effect of light rather than through entrainment of a circadian clock. To resolve this possibility, we evaluated home-cage locomotor activity under constant darkness (D:D or free-running). Activity was tracked using infrared beams for at least 15 d (Figure 3A). We used chi-squared (χ^2) periodograms to estimate period (τ) and also the strength of the activity rhythm as indicated by the % variance explained by the oscillation at the peak period in this test. On average, the period of Kiss1^{ARH}-silenced mice was not different from controls in D:D (Figure 3B; $TeTx_{(n = 5)}$ = 1437 ± 3.74 min, $YFP_{(n=7)}$ = 1431 ± 2.97 min; p = 0.21), although the % variance of the rhythm was significantly weaker (Figure 3A, lower panels for examples; $TeTX_{(n = 5)}$ = 21.8 ± 5.16, $YFP_{(n=7)}$ = 42.88 ± 2.70 min; p = .0028). Kiss1^{ARH}-silenced mice were less active compared to YFP controls ($TeTX_{(n = 5)}$ = 77.9 ± 6.4 vs $YFP_{(n=7)}$ = 110.9 ± 10.0, IR counts per 24 h; p = 0.031), and again this was attributed exclusively to decreased activity during the subjective night (Figures 3C and 3D). Together, these data indicate that Kiss1^{ARH}-neuron signaling promotes physical activity during the D or active phase and, without it, both locomotor and feeding activity are distributed almost equally between L and D phases.

To assess whether decreased locomotor activity of Kiss1^{ARH}-silenced mice was due to a motor impairment, we performed two tests. First, we scored running velocity and distance traveled during a 10-min test in a novel arena. Kiss1^{ARH}-silenced mice traveled a shorter distance during the trial than YFP controls (Figure S2A). Despite suppressed overall activity, Kiss1^{ARH}-silenced mice ran just as fast as controls in this setting, indicating that motor running ability is intact (Figure S2B). Second, we challenged the mice to run and balance on a rotating beam (rotarod) that progressively increased in speed (ramp from 4 to 40 RPM, 2-min trial, 3 trails per day on 3 successive days). Both groups improved their performance

over the 3 testing days and there was no difference in performance between Kiss1^{ARH}-silenced and YFP controls on first trial of each day (Figure S2C). These two tests suggest that Kiss1^{ARH}-silenced mice can balance and move as quickly as control mice; hence, the decreased home-cage and running-wheel activity is unlikely due to a gross motor impairment, but could be due to increased fatigue or decreased motivation to move.

Because Kiss1^{ARH} neurons are important for regulation of GnRH neurons and maintenance of reproductive fitness [23, 25, 26], we predicted that the virally silenced mice would have low levels of estrogen. Although we did not measure estrogen directly, Kiss1^{ARH}-silenced mice had significantly reduced uterine weights (a biological indicator of low estrogen level) compared to YFP-injected controls (dissected at diestrus; 25.51 ± 3.89 g vs 40.27 ± 3.92 g, $p = 0.020$. Student t-test). Importantly, we removed ovarian estrogen by ovariectomy and tested wheel-running activity. Ovariectomy did not change the pattern or amount of daily wheel-running activity in Kiss1^{ARH}-silenced females (Figures S3A-S2B and 2A). Estrogen is generally arousing; numerous studies have found that ovariectomy results in decreased wheel-running locomotor activity [42, 43]. Consistent with this, ovariectomized controls were only ~ 30% as active as gonad-intact controls (Figures S3A, S3C and 2A). Ovariectomized Kiss1^{ARH}-silenced mice displayed less home-cage locomotor activity compared to ovariectomized YFP controls, similar to that observed in intact Kiss1^{ARH}-silenced mice (Figures S3D and 2D). Also, ovariectomy performed 4 wk post TeTx-silencing did not change the body weight trajectory of Kiss1^{ARH}-silenced mice (Figure S3E). These studies indicate that the locomotor and body weight phenotype of Kiss1^{ARH}-silenced mice are independent of ovarian estrogen.

Body temperature (T_b) is under direct circadian regulation and also increases with increased locomotor activity [44-46]. Under a 12:12 h L:D cycle, T_b in mice fluctuates ~2.5 °C between phases (Figures 4A and 4B, segment 1)[47]. Given that home-cage locomotor activity was reduced by ~2 fold during the D phase following Kiss1^{ARH} silencing, we reasoned that this would result in lower D-phase T_b. Telemetry recordings (as shown in Figure 2) simultaneously tracked consecutive days of both activity and temperature. A representative T_b trace from a single mouse is shown in Figure 4A. As anticipated, the average T_b waveform (n = 6; Figure 4B) almost completely paralleled home-cage activity waveforms presented in Figure 2D (same cohort of mice, before and after comparisons). After Kiss1^{ARH} silencing, female mice had a significant decrease in the daily amplitude of Tb (paired t-test of cosinor amplitudes $t_{(5)} = 12.02$: baseline = 1.08 ± 0.09 °C; TeTx = 0.72 ± 0.09 °C; $p < 0.0001$). We evaluated the circadian contribution to the daily T_b oscillation by plotting temperature as a function of activity. Combined analysis of temperature and activity demonstrated that temperature rises within ~10 min of activity bouts (Figure S4). Therefore, we used the sum of activity within a 10-min bin as a predictor of the T_b value at the end of this interval. Equivalent activity levels corresponded with lower T_b values during the L compared to D phase, reflecting a clear circadian contribution to the T_b rhythm, independent of activity (Figure 4C, baseline). Surprisingly, activity-independent T_b was almost completely absent after Kiss1^{ARH} silencing (Figure 4C, TeTx). We rendered a trend line for this observation by ranking activity into 10 defined segments (Figure 4D; described in Supplemental Experimental Procedures). Average T_b within an activity rank was used as a single data point for each animal (n = 6) in both the L and D phases. We attributed the

difference between temperature values in the D versus L as the activity-independent contribution to T_b fluctuations (Figure 4E). These data indicate that the reduced amplitude in the daily oscillation of T_b after TeTx treatment does not represent a sole biproduct of reduced activity levels but also the direct effect of $Kiss1^{ARH}$ silencing on the circadian regulation of temperature.

$Kiss1^{ARH}$ Signaling Is Necessary for Wakefulness during the Night

The Tb and activity rhythm changes along with the diurnal shift in feeding suggests that $Kiss1^{ARH}$-silencing may also affect sleep timing. We implanted electrocorticographic recording electrodes on the cortex along with leads into the dorsal neck to simultaneously monitor brain and muscle activity. Mice were habituated to recording wires and baseline sleep was recorded for 48 h in L:D conditions. We predicted that $Kiss1^{ARH}$-silenced mice would be awake more during the L phase, corresponding with shifted feeding, and that they may compensate for this by sleeping more during the D phase. Similar to feeding patterns, cumulative sleep/wake time over 24-h period was not different between $Kiss1^{ARH}$-silenced and control mice (Figure 5A), but the distribution of sleep and wake in the L:D phases was shifted in $Kiss1^{ARH}$-silenced mice. The average waveform of percent time spent awake demonstrates this shift in $Kiss1^{ARH}$-silenced mice (Figure 5B, left). During the L phase, $Kiss1^{ARH}$-silenced mice were awake for ~1 h longer than YFP controls, but compensated for this by sleeping more during the D phase (Figures 5C and 5B, right). The increase in D-phase sleep was attributed predominantly to slow-wave NREM sleep. We did not detect a change in REM sleep (Figure 5D). In the D phase epochs of total sleep (NREM and REM) were significantly longer in $Kiss1^{ARH}$-silenced versus YFP-injected control mice (mixed-effects survival model with log-rank multiple comparisons: YFP n = 5; TeTx n = 8; $p < 0.001$), while wake epochs were significantly shorter ($p = 0.017$). There was no difference in the length of sleep:wake epochs during the L phase (sleep $p = 0.25$, wake $p = 0.57$). Nocturnal mice sleep predominantly during the L phase and are awake during the D phase. Upon $Kiss1^{ARH}$-silencing there is a shift in distribution sleep/wake making them less nocturnal; a trend that mimics the diurnal shift in feeding behavior (Figure 1).

$Kiss1^{ARH}$ Signaling Does Not Affect Expression of the SCN Clock

Arrhythmic feeding, decreased amplitude rhythms of activity and temperature, and a shift in the timing of sleep stages are consistent with a potential deficit of the master circadian clock in the SCN. Timekeeping properties of cells in the SCN are largely driven by autonomous transcription/translation feedback loops of clock genes [7]. We measured *Per1* expression in the SCN at ZT8 (anticipated peak levels) and ZT16 (anticipated trough levels) with ZT12 being the time lights turn off. There was no difference between *Per1* expression in the SCN of $Kiss1^{ARH}$-silenced and control mice (Figures 6A and 6B). To evaluate regionally distinct cell groups we determined the volume of *Per1* expression along the rostral-caudal and medial-lateral extent of the nucleus (Figure S5). There was no difference of pixel staining throughout the nucleus. Because *Per1* expression in the SCN can be influenced by environmental light and these animals were housed in L:D, our results may not represent endogenous rhythm of the master clock, but rather reflect changes in the light cycle [48]. We designed an experiment to monitor SCN clock-gene expression under D:D conditions using *ex vivo* SCN cultures from $Per2^{luc}$ reporter mice. $Kiss1^{cre}$ mice were crossed to the $Per2^{luc}$

reporter line, and Kiss1^{ARH} neurons were silenced with the TeTx or injected with a control virus as before (Figure 1A). Mice were housed in D:D conditions for at least 10 d, then the SCN was extracted between circadian time (CT) 10 and 11 and luminescence was tracked for 6 d. Representative traces of bioluminescence in the SCN are shown for cultured tissue from YFP and Kiss1^{ARH}-silenced mice (Figure 6C). There was no difference in the circadian period or amplitude of Per2-driven luciferase rhythm in Kiss1^{ARH}-silenced cultures compared to control cultures (Figures 6D and 6E). Overall our results support that Kiss1^{ARH} silencing does not cause an overt change in clock gene expression (Per1 or Per2) in the SCN. Our methods to monitor clock gene expression were not quantitative at the single-cell level and therefore we cannot rule out the possibility that Kiss1^{ARH}-signaling may influence a small subset of SCN time-keeping cells.

Kiss1^{ARH}-silenced mice show dysregulation of the circadian rhythms of feeding, sleep and T_b without changes in overall circadian expression of clock genes in the SCN. This result is consistent with the notion that Kiss1^{ARH} neurons may regulate downstream targets of the SCN to influence the circadian outputs. To get a sense of this possibility, we traced the afferent projections of Kiss1^{ARH} neurons by delivering a conditional virus containing synaptophysin fused to mCherry, AAV1-DIO-Syn:mCherry, into the ARH of *Kiss1^{cre}* mice (Figure 6F). We detected very few Kiss1^{ARH} fibers in the SCN, but identified fibers in the dorsal medial hypothalamus (DMH) and dense projections to the subparaventricular zone (SPZ) dorsal to the SCN (Figure 6G). These data are consistent with previous tracing studies of Kiss1^{ARH} neurons [27]. Interestingly, the DMH and SPZ are downstream relays of the SCN that have been implicated in the circadian regulation of sleep, temperature, and locomotor activity [49-51]. Immunoreactive arginine vasopressin (AVP) and vasoactive intestinal polypeptide (VIP) fibers nicely demonstrate projections from the SCN to the SPZ [52]. We show Kiss1^{ARH} fibers are intermingled with AVP and VIP fibers in the SPZ (Figure S6). Our tracing studies support the notion that Kiss1^{ARH} neurons have sparse terminals within the SCN, but communicate with numerous brain regions downstream of the SCN.

DISCUSSION

To meet the demands of reproduction, neural circuits in female mammals coordinate energy balance and reproductive events. Recent evidence supports the possibility that Kiss1^{ARH} neurons are central to this exchange. Kiss1^{ARH} neurons are a critical component of the neuroendocrine reproductive axis [26], and they communicate information to and from neurons that regulate energy homeostasis. Kiss1^{ARH} neurons are inhibited by orexigenic AgRP neurons in a leptin-dependent manner, likely as a means to gate fertility when energy reserves are low [53, 54]. Conversely, Kiss1^{ARH} neurons feedback to inhibit AgRP neurons, while exciting anorexigenic POMC neurons [30, 31]. Under this scenario, the reproductive state can influence food intake and body weight, likely to assure that sufficient energy is available for reproductive fitness. We hypothesized that chronic silencing of Kiss1^{ARH} neurons would result in increased food intake and weight gain due to the loss of inhibitory tone onto AgRP neurons along with the loss of excitatory tone onto POMC neurons. Kiss1^{ARH}-silenced mice indeed gained a significant amount of weight and were >20% heavier than controls by 8 wk, but surprisingly this weight gain was not attributed to

increased caloric consumption. Rather, Kiss1^{ARH}-silenced female mice were less active and shifted the 24-h timing of feeding and sleep. In the D, Kiss1^{ARH}-silenced mice were less active, ate less, and slept more than control mice. The gain in sleep and decrease feeding during the night were recovered during the L phase, leading to the same amount of food consumption and sleep over a 24-h period in Kiss1^{ARH}-silenced mice compared to controls. These results indicate that the role of Kiss1^{ARH} neurons in the regulation of female metabolism is not simply to determine the amount of food intake but that these cells are also part of the hypothalamic circuitry that times feeding and sleep throughout the day. The arcuate nucleus contains a circadian oscillator [55] and several studies have identified reciprocal synaptic connections between cells in the ARH and the SCN or SCN targets [55-59]. It is likely that Kiss1^{ARH} neurons are not the sole ARH cells that receive information from the SCN. Others have described a role for both leptin-sensitive and Nyp-expressing ARH neurons in locomotor activity rhythms [60, 61]. Our results are consistent with a model in which Kiss1^{ARH} neurons are another key component of an ARH circadian clock that interacts with the hypothalamic circadian circuitry to modulate the amplitude and phase of the rhythms of locomotor activity, sleep, T_b and feeding.

Previous studies have used a variety of techniques to study the necessity of Kiss1 signaling, though none have been specific to Kiss1^{ARH} neurons. Aside from Kiss1^{ARH} neurons, there are other anatomically-distinct Kiss1-expressing cells throughout the brain and in the periphery [62, 63]. Kiss1 receptor knock-out female, but not male, mice are obese, despite consuming less calories than controls [12]. Our results suggest that this phenotype in global Kiss1r knock-out mice could be due to impairment of signaling by Kiss1^{ARH} neurons to their targets. Of note, Kiss1r knock-out females did not show phase-shifted feeding patterns. Kiss1^{ARH} neurons co-express Kiss1, dynorphin, neurokinin B and glutamate [64-66]. The effects that we observe on the timing of feeding in Kiss1^{ARH}-silenced mice could be due to the lack of release of any of these transmitters. Also, it is possible that Kiss1 signaling from distinct populations contribute to unique functions, which might be masked in the global receptor knock-out. Importantly, Kiss1r knock-out mice lack Kiss1 signaling from birth and may develop compensatory adaptations, as has been demonstrated in other hypothalamic cell types such as AgRP neurons [67].

With the goal of studying the influence of Kiss1 neurons on reproduction, one study used a toxin-mediated approach to induce apoptosis in all Kiss1-expressing cells of mice either from birth or induced in adulthood [13]. There was a marginal increase in body weight of females lacking all Kiss1 neurons from birth. The authors did not comment on the circadian activity, temperature or body weight of animals following adult-induced ablation. The Rance laboratory developed a method to ablate *Tacr3*-expressing cells in anatomically-specific brain regions, using a conjugated saporin toxin [68]. This was used as a method to target Kiss1^{ARH} neurons, because they co-express *Tacr3* [65]. Ablation of Tacr3-expressing neurons in the ARH (Tacr3^{ARH}) was sufficient to prevent ovariectomized-induced weight gain in female rats [68]. In contrast,we observed that silencing Kiss1^{ARH} neurons resulted in weight gain compared to controls, and was not altered by ovariectomy. Also, unlike Tacr3^{ARH}-ablated rats, we found a significant reduction in the amplitude of T_b following Kiss1^{ARH} silencing. Importantly, most Kiss1^{ARH} neurons express *Tacr3*; however, *Tacr3*

does not appear to be specific to Kiss1^{ARH} neurons and the strategy may ablate non-Kiss1^{ARH} neurons [65].

A recent study in rats found that severing axonal connections between the SCN and ARH profoundly suppressed both locomotor and T_b amplitude without affecting clock-gene expression within the SCN [69]. Similarly, clock-gene expression was not affected in Kiss1^{ARH}-silenced mice in our study. Together, these results suggest that Kiss1^{ARH} neurons do not directly regulate the circadian molecular machinery of SCN cells but instead regulate SCN input to its targets either by axo-axonal connections to SCN efferents or through converging input to neurons innervated by the SCN. Accordingly, we did not detect direct Kiss1^{ARH} projections to the SCN but identified dense projections from Kiss1^{ARH} neurons to the SPZ and DMH, both SCN targets that have been implicated in the regulation of circadian rhythms in locomotor activity, temperature and sleep [50, 51].

We show that Kiss1^{ARH} neurons are a necessary component of circadian T_b fluctuations. This is an exciting finding because of work supporting the idea that circadian T_b fluctuations provide a master-clock-driven cue to entrain (or synchronize) peripheral oscillators throughout the brain and body [11, 70]. Kiss1^{ARH} neurons may therefore orchestrate circadian outcomes via thermoregulation. Previously, we and others have shown that Kiss1^{ARH} neurons are involved in sex-hormone-mediated thermoregulation via neurokinin B signaling to heat-effector cells in the preoptic area of the hypothalamus [27-29]. It is possible that this same relay is involved in the circadian regulation of Tb and that it can either be triggered by time-of-day or sex-hormone cues controlling the activity of Kiss1^{ARH} neurons.

Because Kiss1^{ARH} neurons are controlled by both gonadal hormones and energy status, they may offer insights into sex- and nutrient-mediated circadian disruptions. The activity of Kiss1^{ARH} neurons, as measured by *Fos* and the expression of both *Kiss1* and *Tac2* mRNAs within these neurons, is negatively regulated by both estrogen and testosterone [14, 17, 71-73]. In females, many circadian rhythms are influenced by the estrogen state. Rodents demonstrate a phase-advance in locomotor activity on the day of estrus and a shortened free-running period when administered a chronic, high dose of estrogen [74]. In the absence of ovarian estrogen, female rodents are less active on a free-access running wheel [42, 43, 75]. The daily oscillation of T_b also shows distinct changes throughout the estrous cycle and pregnancy [47, 76, 77]. Sleep architecture is also influenced by estrogen state. In humans, NREM slow-wave sleep has a menstrual rhythm with higher percent (of total sleep) during the luteal phase compared with the follicular phase of the estrous cycle [76, 78]. Female mice sleep less during the night of proestrus, when estrogen is high [79]. Importantly, the SCN does not directly sense estrogen [80]; thus, Kiss1^{ARH} neurons may provide a means by which sex hormones can influence the SCN clock-mediated functions. Aside from sex hormones, Kiss1^{ARH} neuron activity is also regulated by energy status via synaptic input from AgRP neurons, a connection that serves to gate fertility when energy balance is low [53]. AgRP neurons are activated during chronic caloric restriction, such as in anorexia nervosa, and patients suffering from anorexia have comorbid sleep disruptions [81]. Anorexia may therefore mimic the sleep profile that we observe in Kiss1^{ARH}-silenced mice. In summary, Kiss1^{ARH} neurons in females are at a nodal position to integrate reproductive

and energy status. Our results suggest that they also represent a key source of circadian activation/inhibition that modulate the timing of physiological and behavioral processes. Contemporary tools provide a means to gain control of and manipulate genetically defined Kiss1 neurons in a reversible fashion. Phase-specific manipulation of $Kiss1^{ARH}$ neurons in the context of specific hormone or nutrient states is an exciting arena for future work.

STAR★Methods

Contact for Reagent and Resource Sharing

Further information and requests should be directed to and will be fulfilled by the Lead Contact, Stephanie L. Padilla (slpadilla@umass.edu)

Experimental Model and Subject Details

Animals—These experiments were performed with approval from the University of Washington's Animal Care and Use Committee, in accordance with the NIH Guide for care and use of laboratory animals. Adult female mice, ages 2-8 months, had *ad libitum* access to food (standard chow, or Research Diet's D12450B for BioDaq food intake monitoring) and water. The light cycle is indicated for specific experiments in this manuscript. Zeitgeber time zero (ZT0) indicates the onset of the light cycle, and circadian time zero (CT0) indicates the onset of the rest phase in constant darkness. We used two mouse transgenic mouse lines in this manuscript. 1) $Kiss1^{cre:GFP}$ (version 2 with attenuated Cre expression, referred to as $Kiss1^{cre}$) knock-in mice that were generated in our lab and previously characterized [29]. Homozygous $Kiss1^{Cre/Cre}$ mice are infertile and hence we used heterozygous breeders and heterozygous $Kiss1^{Cre/+}$ mice for all experiments in this manuscript. 2) $Per2^{luc}$ transgenic knock-in mice were engineered to express the luciferase reporter as a fusion protein with the functional *Per2* clock gene [9]. These mice were generously given to us by the laboratory of Dr. Ethan Burh at the University of Washington.

Method Details

Viruses and stereotactic injections—$Kiss1^{cre}$ mice received bilateral injections of an adeno-associated virus (AAV, serotype 1) containing a conditional transgene. The following viruses were prepared at the University of Washington [82]: AAV1-CBA-DIO-GFP:TeTx, AAV1-Ef1α-DIO-YFP, AAV1-Ef1α-DIO-Synaptophysin:mCh, AAV1-Eftα-DIO-Synaptophysin:GFP. 500 nl of virus was injected at a working concentration of ~10^9 particles/ml to each hemisphere of the arcuate nucleus of the hypothalamus. Targeted injections were performed aseptically, while head-fixed on a stereotaxic device and anesthetized with 2% isoflurane/O_2. Our injection coordinates for the ARH were: −1.25 mm (bregma), −5.8 mm (ventral), ± 0.3 mm (lateral). Viruses were loaded into pulled glass capillary needles that were backfilled with biologically inert Perfluro-compound (FC-770) and administered using a Nanoject ii (Drummond Scientific) that was fit to the stereotaxic frame.

Activity

Wheel-running: Wheel turns were monitored by two opposing magnetic sensors on the home-cage running wheel. Sensor counts were tracked with AltiMetrics ClockLab (Wilmette, IL).

Home cage activity and body temperature: Home-cage activity was monitored by either infrared beam (IR) breaks or telemetry with an implanted intraperitoneal transponder and corresponding receiver. We used two methods of IR tracking. 1) Columbus Instruments, Opto-Max Activity Meter (Figure S3D). The home cage was placed between 4 external sensors. Recordings started after 6 h of habituation to the room and environment and activity was gathered for 48 h. Data were gathered with Opto-Max software and raw activity values were exported and processed in Excel. 2) A small motion detector (RS components, Gardtec Gardscan QX detector, CCCN 85311030) was placed in the animal's home cage and connected to Altmetrics Clocklab to record beam breaks (Figure 3).

Telemetry recordings were performed using Starr's G2 E-mitter Telemetry system. Following surgical implantation of the transponder, animals recovered for at least 2 wk prior to recording. The home cage was placed on an ER4000 receiver and both activity and T_b was measured every minute (counts tracked with VitalView). 20-min T_b averages were calculated for 3 successive days and used to construct 24h T_b waveforms (Figure 4B). To assess the effect of activity-generated heat on T_b we analyzed each single T_b value as a function of the sum of activity 10 min prior to this time point. Three d of T_b and activity values are plotted in Figure 4C and divided into light and dark phases. To determine the circadian contribution to the daily T_b oscillations, activity values were binned into a rank order (Figure 4D x-axis: 1 = 0-49, 2 = 50-149, 3 = 150-249, 4 = 250-349, 5 = 350-449, 6 = 450-549, 7=550-649, 8 = 650-749, 9 = 750-849, 10 = 850-949 units of activity). For each animal, we calculated the average Tb within each activity rank so that each animal generated a single T_b value per rank point; Fig. 4D shows the mean ± SEM for all the animals. We subtracted the T_b values at each rank point within the indicated square (rank points 2-7) between the light and dark phases. This was done for each animal individually, before and after TeTx, and the averaged difference values are compared in Figure 4E.

Raw data were converted into double-plotted actograms using El Temps software, or processed and binned in Excel and plotted using Prism software (Graphpad). El Temps was used for Cosinor analysis.

Rotarod: Latency to fall from a rotating rod (Rotamex 4/8, Columbus Instruments) was assessed over 3 consecutive days with three trails per day. Daily trails were performed during the light phase and had an ITI of 20 min. The rod accelerated from 4-40 RPM over a 2-min trial [83].

Open field: Mice were positioned facing the wall of a novel cylindrical arena (56 inches in diameter). Locomotor movement was videotaped (10-min trial during the light phase). Trace measurements of distance and velocity were determined by Noldus EthoVision [84].

Feeding—BioDAQ food monitoring system was used to track feeding patterns. Feeding counts were tracked with DataViewer software. Feedograms were constructed from the raw data using El Temps software.

Histology

In situ hybridization (ISH): All ISH procedures were performed on 10 mm-fresh-frozen coronal sections on slides. Mice were euthanized by decapitation, the brain was quickly dissected and flash frozen in 2-methal butane at - 30°C. Fresh-frozen tissue was stored at −80°C until cyro-sectioning.

Radiolabeled ISH for Per1: Animals from each cohort (YFP-injected controls and Kiss1-^{ARH}-silenced mice) were divided into two groups and sacrificed at either ZT8 or ZT16. A radiolabeled antisense RNA probe was transcribed from *Per1* cDNA using ^{35}S-UTP. The probe (10^8 cpm/ml) was hybridized onto slide-adhered tissue, 55°C for 12 h [85]. Radiolabeled *ISH* signals were developed on film and scanned with a high resolution scanner (Silverfast Microtek 8700).

RNAscope ISH: The Multiplex Fluorescent Detection Kit v2 kit was performed as recommended (Advanced Cell Diagnostic, 323110) using probes against *Kiss1* (ACD, 476291-C3) and *TeTx* (ACD, 300031-C2).

Immunohistochemistry: Mice were euthanized with Beuthanasia-D Special (effective dose 320 mg/kg pentobarbital) and transcardially perfused with cold saline, followed by 4% paraformaldehyde 0.1 M phosphate buffer (PFA). Brains were post-fixed in PFA (overnight, 4°C), and then cryopreserved by incubation in cold 30% sucrose solution until sinking. Brains were then flash frozen and stored at −80°C (described for *ISH* preparation). Coronal cryo-sections were prepared in PBS and processed within 1 week of sectioning. Sections were first blocked for 1 hour, room temperature (0.2% Triton X-100 and 3% donkey serum in PBS). Sections were then exposed to the primary antibody (4°C overnight) and the next day were incubated with a corresponding secondary antibody (2 h, RT). Primary antibodies: rabbit anti-DsRed (Clontech 632496; diluted 1:1000), rabbit anti-GFP (Invitrogen A11122), chicken anti-GFP (Abcam 13970), guinea pig anti-VIP (Peninsula Lab, T5030.0050), rabbit anti-AVP (Chemicon International, 24030226). Processed sections were mounted onto glass slides and coverslipped with DAPI Fluoromount-G (Southern Biotech, 0100-290). Images were acquired with a slide-scanning microscope (Keyence, BZ-X710).

EcOG/EMG recordings

Implant: Electrodes (Pinnacle 8209), tethered to a 6-pin IC component socket board (Max-Mill 853-93-100-10-001000), were implanted in the primary motor cortex at positions (bregma/lateral): EcOG-1, +0.3/+1.6; EcOG-2, +0.3/−1.6; reference, −6.0/−1.5; ground, −4.0/1.5; and cemented to the skull. Two leads (silver wire, A-M Systems 78700) from the socket board were routed to the dorsal neck muscles for EMG recordings. Animals recovered from the implant surgery for ≥ 1 wk prior to sleep recordings.

Data acquisition: Animals were placed in a sleep-recording chamber and tethered to the recording apparatus (Pinnacle). EcOG signals were collected at 128-Hz and recorded in 10-sec epochs. Following a 9 h acclimation to the tether and housing, 2 d of electrical activity was recorded under a 12:12 h light:dark cycle.

Scoring: A trained user manually-scored 3 h of sleep recording (ZT 7–10), as described [86]. Wake state was characterized by fast low-amplitude ECoG waves with EMG muscle activity. Sleep was divided into two categories: NREM sleep was characterized by slow, high-amplitude delta waves (power frequency between 0.5-4 Hz) with low muscle activity, whereas REM sleep was characterized by fast low-amplitude theta waves (power frequency between 6-12 Hz) and muscle paralysis. Manual scores were assigned to 10-s epochs, for 3 h during the final third of the light phase; a time window with the highest probability to detect both stages of sleep, along with wake states. Next, we processed recordings during this same time interval using an autoscoring algorithm that was written in R (version 3.3.0) and described previously [87]. Manual scores were used as a standard to validate the autoscoring algorithm. Animals were excluded if there was not ≥ 85% agreement between the autoscoring and manual scores. Once validated, the autoscoring algorithm was used to score 2 d of recordings for each animal. Note, two animals were excluded from the study due to either noisy recordings that could not be resolved for scoring or because they did not meet the autoscoring criteria.

Per2^{Luc} rhythms

Data acquisition: *Kiss1*^{cre};*Per2*^{Luc} reporter mice were housed in constant darkness (activity tracked with IR motion sensor) for at least 10 d prior to tissue collection. At ~CT 10-11 mice were euthanized via rapid decapitation, brain were dissected into freezing HBSS (Thermo Fisher Scientific, 14185052) and a 300 mm coronal slice of the SCN was prepared on a vibratome. Sections containing the SCN were placed on 0.4 cell culture inserts (Millipore, PICM0RG50) in sealed 35 mm Petri dishes (Thermo Fisher Scientific, 150318) containing 1.2 ml of DMEM (Corning, 90-013-PB) supplemented with B-27 supplement (Thermo Fisher Scientific, 17504044), 352.5 μg/mL sodium bicarbonate (Thermo Fisher Scientific, 25080094), 10 mM Hepes (Thermo Fisher Scientific, 15630080), 25 U/mL penicillin, 25 μg/mL streptomycin (Thermo Fisher Scientific, 15140148), Glutamax (Thermo Fisher Scientific, 35050061) and 0.1 mM luciferin potassium salt (Gold Biotechnology, 115144-35-9). SCN explants were incubated at 36°C and images were acquired every 30 min (29 min exposure) for 6 d (Pixis 1024 X 1024 camera, Princeton Instruments).

Data processing: Pixel intensity of luciferace bioluminescence in the SCN was converted to digital values using ImageJ ROI manager. To detrend the raw data and remove the baseline drift, we subtracted the 24 h running mean.

Fertility assays

Uterine weight: To standardize the measurements, dissections were performed on diestrus when the vaginal fluid contained predominantly leucocyte cells (vaginal lavage with saline).

The uterus was dissected and the horns were trimmed to ±1 cm from the center point [88, 89].

Estrous cycle: Animals were single-housed and handled exclusively by the investigator during this study. Within 2 h of the light phase, a vaginal lavage sample was collected in sterile PBS. Samples on slides were evaluated for the presence of leukocytes, cornified epithelial cells, and nucleated epithelial cells. Proestrus was scored when the sample contained predominantly nucleated epithelial cells with a near to complete loss of leukocytes. Samples containing primarily cornified epithelial cells were scored as estrus.

Luteinizing hormone (LH) ultra-sensitive ELISA: Following estrous cycle tracking, we evaluated serum LH at diestrus. 6 μl of blood was collected from the tail at 5-min intervals for 45 min (tail tips were clipped 30 min before sample collection). Whole blood samples were diluted in 114 μl of assay buffer (0.1 M PBS with 0.2% BSA and 0.05% Tween 20) and stored at −80°C until processing. ELISA was performed by the Center for Research in Reproduction Ligand Core at the University of Virginia.

Quantification and Statistical analysis

Data Analysis

Statistics were calculated with Prism software from GraphPad. Each figure legend contains full statistical reports for each comparison. The thresholds for p value significance are: *$p < 0.05$, **$p < 0.01$, and ***$p < 0.001$). All error bars represent the standard error of the mean.

Survival analysis of sleep

First, we identified all periods consisting of contiguous epochs of a specific stage (either ‘wake’, ‘total sleep’ (REM & NREM), ‘REM’, or ‘NREM’). After we identified all periods of contiguous sleep/wake in each mouse, we pooled all data from all mice in a single treatment group and generated two survival curves by using a Cox proportional hazards regression model with mixed effects using mouse ID as a random factor nested within treatment group. Each group survival curve characterizes the overall distribution of sleep/wake bout lengths for all subjects for a single treatment group. All analyses were done with R version 3.3.0 using the ‘survival’ and ‘coxme’ packages.

Supplementary Material

Refer to Web version on PubMed Central for supplementary material.

ACKNOWLEDGMENTS

We thank all of the member of the Palmiter and de la Iglesia labs for thoughtful discussions of this work. We thank Megan Chiang, Kathy Kafer, Natassya West, Luis Salazar and Tenley Weil for assistance with animal work. We thank Dr. James Allen for synthesizing the viruses used in this manuscript.

REFERENCES

1. Acosta-Rodriguez VA, de Groot MHM, Rijo-Ferreira F, Green CB, and Takahashi JS (2017). Mice under Caloric Restriction Self-Impose a Temporal Restriction of Food Intake as Revealed by an Automated Feeder System. Cell Metab 26, 267–277 e262. [PubMed: 28683292]
2. Arble DM, Bass J, Laposky AD, Vitaterna MH, and Turek FW (2009). Circadian timing of food intake contributes to weight gain. Obesity (Silver Spring) 17, 2100–2102. [PubMed: 19730426]
3. Hatori M, Vollmers C, Zarrinpar A, DiTacchio L, Bushong EA, Gill S, Leblanc M, Chaix A, Joens M, Fitzpatrick JA, et al. (2012). Time-restricted feeding without reducing caloric intake prevents metabolic diseases in mice fed a high-fat diet. Cell Metab 15, 848–860. [PubMed: 22608008]
4. Wang F, Zhang L, Zhang Y, Zhang B, He Y, Xie S, Li M, Miao X, Chan EY, Tang JL, et al. (2014). Meta-analysis on night shift work and risk of metabolic syndrome. Obes Rev 15, 709–720. [PubMed: 24888416]
5. Mattson MP, Allison DB, Fontana L, Harvie M, Longo VD, Malaisse WJ, Mosley M, Notterpek L, Ravussin E, Scheer FA, et al. (2014). Meal frequency and timing in health and disease. Proc Natl Acad Sci U S A 111, 16647–16653. [PubMed: 25404320]
6. Hastings MH, Maywood ES, and Brancaccio M (2018). Generation of circadian rhythms in the suprachiasmatic nucleus. Nat Rev Neurosci.
7. Mohawk JA, Green CB, and Takahashi JS (2012). Central and peripheral circadian clocks in mammals. Annu Rev Neurosci 35, 445–462. [PubMed: 22483041]
8. LeGates TA, Fernandez DC, and Hattar S (2014). Light as a central modulator of circadian rhythms, sleep and affect. Nature Reviews Neuroscience 15, 443–454. [PubMed: 24917305]
9. Yoo SH, Yamazaki S, Lowrey PL, Shimomura K, Ko CH, Buhr ED, Siepka SM, Hong HK, Oh WJ, Yoo OJ, et al. (2004). PERIOD2::LUCIFERASE real-time reporting of circadian dynamics reveals persistent circadian oscillations in mouse peripheral tissues. Proc Natl Acad Sci U S A 101, 5339–5346. [PubMed: 14963227]
10. Mure LS, Le HD, Benegiamo G, Chang MW, Rios L, Jillani N, Ngotho M, Kariuki T, Dkhissi-Benyahya O, Cooper HM, et al. (2018). Diurnal transcriptome atlas of a primate across major neural and peripheral tissues. Science 359.
11. Buhr ED, Yoo SH, and Takahashi JS (2010). Temperature as a universal resetting cue for mammalian circadian oscillators. Science 330, 379–385. [PubMed: 20947768]
12. Tolson KP, Garcia C, Yen S, Simonds S, Stefanidis A, Lawrence A, Smith JT, and Kauffman AS (2014). Impaired kisspeptin signaling decreases metabolism and promotes glucose intolerance and obesity. J Clin Invest 124, 3075–3079. [PubMed: 24937427]
13. Mayer C, and Boehm U (2011). Female reproductive maturation in the absence of kisspeptin/GPR54 signaling. Nat Neurosci 14, 704–710. [PubMed: 21516099]
14. Smith JT, Cunningham MJ, Rissman EF, Clifton DK, and Steiner RA (2005). Regulation of Kiss1 gene expression in the brain of the female mouse. Endocrinology 146, 3686–3692. [PubMed: 15919741]
15. Clarkson J, d'Anglemont de Tassigny X, Moreno AS, Colledge WH, and Herbison AE (2008). Kisspeptin-GPR54 signaling is essential for preovulatory gonadotropin-releasing hormone neuron activation and the luteinizing hormone surge. J Neurosci 28, 8691–8697. [PubMed: 18753370]
16. Piet R, Kalil B, McLennan T, Porteous R, Czieselsky K, and Herbison AE (2018). Dominant Neuropeptide Cotransmission in Kisspeptin-GABA Regulation of GnRH Neuron Firing Driving Ovulation. J Neurosci 38, 6310–6322. [PubMed: 29899026]
17. Smith JT, Dungan HM, Stoll EA, Gottsch ML, Braun RE, Eacker SM, Clifton DK, and Steiner RA (2005). Differential regulation of KiSS-1 mRNA expression by sex steroids in the brain of the male mouse. Endocrinology 146, 2976–2984. [PubMed: 15831567]
18. Legan SJ, and Karsch FJ (1975). A daily signal for the LH surge in the rat. Endocrinology 96, 57–62. [PubMed: 1167356]
19. Stetson MH, Watson-Whitmyre M, Dipinto MN, and Smith SG 3rd (1981). Daily luteinizing hormone release in ovariectomized hamsters: effect of barbiturate blockade. Biol Reprod 24, 139–144. [PubMed: 7470539]

20. Williams WP 3rd, Jarjisian SG, Mikkelsen JD, and Kriegsfeld LJ (2011). Circadian control of kisspeptin and a gated GnRH response mediate the preovulatory luteinizing hormone surge. Endocrinology 152, 595–606. [PubMed: 21190958]
21. Smarr BL, Gile JJ, and de la Iglesia HO (2013). Oestrogen-independent circadian clock gene expression in the anteroventral periventricular nucleus in female rats: possible role as an integrator for circadian and ovarian signals timing the luteinising hormone surge. J Neuroendocrinol 25, 1273–1279. [PubMed: 24028332]
22. Piet R, Fraissenon A, Boehm U, and Herbison AE (2015). Estrogen permits vasopressin signaling in preoptic kisspeptin neurons in the female mouse. J Neurosci 35, 6881–6892. [PubMed: 25926463]
23. Qiu J, Nestor CC, Zhang CG, Padilla SL, Palmiter RD, Kelly MJ, and Ronnekleiv OK (2016). High-frequency stimulation-induced peptide release synchronizes arcuate kisspeptin neurons and excites GnRH neurons. Elife 5.
24. Han SY, McLennan T, Czieselsky K, and Herbison AE (2015). Selective optogenetic activation of arcuate kisspeptin neurons generates pulsatile luteinizing hormone secretion. Proc Natl Acad Sci U S A 112, 13109–13114. [PubMed: 26443858]
25. Clarkson J, Han SY, Piet R, McLennan T, Kane GM, Ng J, Porteous RW, Kim JS, Colledge WH, Iremonger KJ, et al. (2017). Definition of the hypothalamic GnRH pulse generator in mice. Proc Natl Acad Sci U S A 114, E10216–E10223. [PubMed: 29109258]
26. Mittelman-Smith MA, Krajewski-Hall SJ, McMullen NT, and Rance NE (2016). Ablation of KNDy Neurons Results in Hypogonadotropic Hypogonadism and Amplifies the Steroid-Induced LH Surge in Female Rats. Endocrinology 157, 2015–2027. [PubMed: 26937713]
27. Yeo SH, and Herbison AE (2011). Projections of arcuate nucleus and rostral periventricular kisspeptin neurons in the adult female mouse brain. Endocrinology 152, 2387–2399. [PubMed: 21486932]
28. Mittelman-Smith MA, Williams H, Krajewski-Hall SJ, McMullen NT, and Rance NE (2012). Role for kisspeptin/neurokinin B/dynorphin (KNDy) neurons in cutaneous vasodilatation and the estrogen modulation of body temperature. Proc Natl Acad Sci U S A 109, 19846–19851. [PubMed: 23150555]
29. Padilla SL, Johnson CW, Barker FD, Patterson MA, and Palmiter RD (2018). A Neural Circuit Underlying the Generation of Hot Flushes. Cell Rep 24, 271–277. [PubMed: 29996088]
30. Fu LY, and van den Pol AN (2010). Kisspeptin directly excites anorexigenic proopiomelanocortin neurons but inhibits orexigenic neuropeptide Y cells by an indirect synaptic mechanism. J Neurosci 30, 10205–10219. [PubMed: 20668204]
31. Nestor CC, Qiu J, Padilla SL, Zhang C, Bosch MA, Fan W, Aicher SA, Palmiter RD, Ronnekleiv OK, and Kelly MJ (2016). Optogenetic Stimulation of Arcuate Nucleus Kiss1 Neurons Reveals a Steroid-Dependent Glutamatergic Input to POMC and AgRP Neurons in Male Mice. Mol Endocrinol 30, 630–644. [PubMed: 27093227]
32. Yu CR, Power J, Barnea G, O'Donnell S, Brown HE, Osborne J, Axel R, and Gogos JA (2004). Spontaneous neural activity is required for the establishment and maintenance of the olfactory sensory map. Neuron 42, 553–566. [PubMed: 15157418]
33. Heimer-McGinn V, Murphy AC, Kim JC, Dymecki SM, and Young PW (2013). Decreased dendritic spine density as a consequence of tetanus toxin light chain expression in single neurons in vivo. Neurosci Lett 555, 36–41. [PubMed: 24035894]
34. Han S, Soleiman MT, Soden ME, Zweifel LS, and Palmiter RD (2015). Elucidating an Affective Pain Circuit that Creates a Threat Memory. Cell 162, 363–374. [PubMed: 26186190]
35. Campos CA, Bowen AJ, Schwartz MW, and Palmiter RD (2016). Parabrachial CGRP Neurons Control Meal Termination. Cell Metab 23, 811–820. [PubMed: 27166945]
36. Campos CA, Bowen AJ, Han S, Wisse BE, Palmiter RD, and Schwartz MW (2017). Cancer-induced anorexia and malaise are mediated by CGRP neurons in the parabrachial nucleus. Nat Neurosci 20, 934–942. [PubMed: 28581479]
37. Casiraghi LP, Alzamendi A, Giovambattista A, Chiesa JJ, and Golombek DA (2016). Effects of chronic forced circadian desynchronization on body weight and metabolism in male mice. Physiol Rep 4.

38. Turek FW, Joshu C, Kohsaka A, Lin E, Ivanova G, McDearmon E, Laposky A, Losee-Olson S, Easton A, Jensen DR, et al. (2005). Obesity and metabolic syndrome in circadian Clock mutant mice. Science 308, 1043–1045. [PubMed: 15845877]
39. Coomans CP, van den Berg SA, Lucassen EA, Houben T, Pronk AC, van der Spek RD, Kalsbeek A, Biermasz NR, Willems van Dijk K, Romijn JA, et al. (2013). The suprachiasmatic nucleus controls circadian energy metabolism and hepatic insulin sensitivity. Diabetes 62, 1102–1108. [PubMed: 23274903]
40. Pierce WD, Epling WF, and Boer DP (1986). Deprivation and Satiation - the Interrelations between Food and Wheel Running. J Exp Anal Behav 46, 199–210. [PubMed: 16812460]
41. Hsu YW, Wang SD, Wang S, Morton G, Zariwala HA, de la Iglesia HO, and Turner EE (2014). Role of the dorsal medial habenula in the regulation of voluntary activity, motor function, hedonic state, and primary reinforcement. J Neurosci 34, 11366–11384. [PubMed: 25143617]
42. Gentry RT, and Wade GN (1976). Sex differences in sensitivity of food intake, body weight, and running-wheel activity to ovarian steroids in rats. J Comp Physiol Psychol 90, 747–754. [PubMed: 965523]
43. Iwahana E, Karatsoreos I, Shibata S, and Silver R (2008). Gonadectomy reveals sex differences in circadian rhythms and suprachiasmatic nucleus androgen receptors in mice. Horm Behav 53, 422–430. [PubMed: 18164002]
44. Refinetti R (1994). Contribution of locomotor activity to the generation of the daily rhythm of body temperature in golden hamsters. Physiol Behav 56, 829–831. [PubMed: 7800756]
45. Scheer FA, Pirovano C, Van Someren EJ, and Buijs RM (2005). Environmental light and suprachiasmatic nucleus interact in the regulation of body temperature. Neuroscience 132, 465–477. [PubMed: 15802197]
46. Cambras T, Weller JR, Angles-Pujoras M, Lee ML, Christopher A, Diez-Noguera A, Krueger JM, and de la Iglesia HO (2007). Circadian desynchronization of core body temperature and sleep stages in the rat. Proc Natl Acad Sci U S A 104, 7634–7639. [PubMed: 17452631]
47. Sanchez-Alavez M, Alboni S, and Conti B (2011). Sex- and age-specific differences in core body temperature of C57Bl/6 mice. Age (Dordr) 33, 89–99. [PubMed: 20635153]
48. Golombek DA, and Rosenstein RE (2010). Physiology of circadian entrainment. Physiol Rev 90, 1063–1102. [PubMed: 20664079]
49. Watts AG, Swanson LW, and Sanchez-Watts G (1987). Efferent projections of the suprachiasmatic nucleus: I. Studies using anterograde transport of Phaseolus vulgaris leucoagglutinin in the rat. J Comp Neurol 258, 204–229. [PubMed: 3294923]
50. Lu J, Zhang YH, Chou TC, Gaus SE, Elmquist JK, Shiromani P, and Saper CB (2001). Contrasting effects of ibotenate lesions of the paraventricular nucleus and subparaventricular zone on sleep-wake cycle and temperature regulation. J Neurosci 21, 4864–4874. [PubMed: 11425913]
51. Saper CB, Lu J, Chou TC, and Gooley J (2005). The hypothalamic integrator for circadian rhythms. Trends Neurosci 28, 152–157. [PubMed: 15749169]
52. Vujovic N, Gooley JJ, Jhou TC, and Saper CB (2015). Projections from the subparaventricular zone define four channels of output from the circadian timing system. J Comp Neurol 523, 2714–2737. [PubMed: 26010698]
53. Padilla SL, Qiu J, Nestor CC, Zhang C, Smith AW, Whiddon BB, Ronnekleiv OK, Kelly MJ, and Palmiter RD (2017). AgRP to Kiss1 neuron signaling links nutritional state and fertility. Proc Natl Acad Sci U S A 114, 2413–2418. [PubMed: 28196880]
54. Egan OK, Inglis MA, and Anderson GM (2017). Leptin Signaling in AgRP Neurons Modulates Puberty Onset and Adult Fertility in Mice. J Neurosci 37, 3875–3886. [PubMed: 28275162]
55. Abe M, Herzog ED, Yamazaki S, Straume M, Tei H, Sakaki Y, Menaker M, and Block GD (2002). Circadian rhythms in isolated brain regions. J Neurosci 22, 350–356. [PubMed: 11756518]
56. Horvath TL (1997). Suprachiasmatic efferents avoid phenestrated capillaries but innervate neuroendocrine cells, including those producing dopamine. Endocrinology 138, 1312–1320. [PubMed: 9048641]
57. Saeb-Parsy K, Lombardelli S, Khan FZ, McDowall K, Au-Yong IT, and Dyball RE (2000). Neural connections of hypothalamic neuroendocrine nuclei in the rat. J Neuroendocrinol 12, 635–648. [PubMed: 10849208]

58. Guilding C, Hughes AT, Brown TM, Namvar S, and Piggins HD (2009). A riot of rhythms: neuronal and glial circadian oscillators in the mediobasal hypothalamus. Mol Brain 2, 28. [PubMed: 19712475]
59. Guzman-Ruiz MA, Ramirez-Corona A, Guerrero-Vargas NN, Sabath E, Ramirez-Plascencia OD, Fuentes-Romero R, Leon-Mercado LA, Basualdo Sigales M, Escobar C, and Buijs RM (2015). Role of the Suprachiasmatic and Arcuate Nuclei in Diurnal Temperature Regulation in the Rat. J Neurosci 35, 15419–15429. [PubMed: 26586828]
60. Li AJ, Wiater MF, Oostrom MT, Smith BR, Wang Q, Dinh TT, Roberts BL, Jansen HT, and Ritter S (2012). Leptin-sensitive neurons in the arcuate nuclei contribute to endogenous feeding rhythms. Am J Physiol Regul Integr Comp Physiol 302, R1313–1326. [PubMed: 22492818]
61. Wiater MF, Mukherjee S, Li AJ, Dinh TT, Rooney EM, Simasko SM, and Ritter S (2011). Circadian integration of sleep-wake and feeding requires NPY receptor-expressing neurons in the mediobasal hypothalamus. Am J Physiol Regul Integr Comp Physiol 301, R1569–1583. [PubMed: 21880863]
62. Bhattacharya M, and Babwah AV (2015). Kisspeptin: beyond the brain. Endocrinology 156, 1218–1227. [PubMed: 25590245]
63. Stephens SBZ, and Kauffman AS (2017). Regulation and Possible Functions of Kisspeptin in the Medial Amygdala. Front Endocrinol (Lausanne) 8, 191. [PubMed: 28824550]
64. Goodman RL, Lehman MN, Smith JT, Coolen LM, de Oliveira CV, Jafarzadehshirazi MR, Pereira A, Iqbal J, Caraty A, Ciofi P, et al. (2007). Kisspeptin neurons in the arcuate nucleus of the ewe express both dynorphin A and neurokinin B. Endocrinology 148, 5752–5760. [PubMed: 17823266]
65. Navarro VM, Gottsch ML, Chavkin C, Okamura H, Clifton DK, and Steiner RA (2009). Regulation of gonadotropin-releasing hormone secretion by kisspeptin/dynorphin/neurokinin B neurons in the arcuate nucleus of the mouse. J Neurosci 29, 11859–11866. [PubMed: 19776272]
66. Cravo RM, Margatho LO, Osborne-Lawrence S, Donato J Jr., Atkin S, Bookout AL, Rovinsky S, Frazao R, Lee CE, Gautron L, et al. (2011). Characterization of Kiss1 neurons using transgenic mouse models. Neuroscience 173, 37–56. [PubMed: 21093546]
67. Luquet S, Perez FA, Hnasko TS, and Palmiter RD (2005). NPY/AgRP neurons are essential for feeding in adult mice but can be ablated in neonates. Science 310, 683–685. [PubMed: 16254186]
68. Mittelman-Smith MA, Williams H, Krajewski-Hall SJ, Lai J, Ciofi P, McMullen NT, and Rance NE (2012). Arcuate kisspeptin/neurokinin B/dynorphin (KNDy) neurons mediate the estrogen suppression of gonadotropin secretion and body weight. Endocrinology 153, 2800–2812. [PubMed: 22508514]
69. Buijs FN, Guzman-Ruiz M, Leon-Mercado L, Basualdo MC, Escobar C, Kalsbeek A, and Buijs RM (2017). Suprachiasmatic Nucleus Interaction with the Arcuate Nucleus; Essential for Organizing Physiological Rhythms. eNeuro 4.
70. Reinke H, Saini C, Fleury-Olela F, Dibner C, Benjamin IJ, and Schibler U (2008). Differential display of DNA-binding proteins reveals heat-shock factor 1 as a circadian transcription factor. Genes Dev 22, 331–345. [PubMed: 18245447]
71. Ciofi P, Krause JE, Prins GS, and Mazzuca M (1994). Presence of nuclear androgen receptor-like immunoreactivity in neurokinin B-containing neurons of the hypothalamic arcuate nucleus of the adult male rat. Neurosci Lett 182, 193–196. [PubMed: 7715808]
72. Goubillon ML, Forsdike RA, Robinson JE, Ciofi P, Caraty A, and Herbison AE (2000). Identification of neurokinin B-expressing neurons as an highly estrogen-receptive, sexually dimorphic cell group in the ovine arcuate nucleus. Endocrinology 141, 4218–4225. [PubMed: 11089556]
73. Burke MC, Letts PA, Krajewski SJ, and Rance NE (2006). Coexpression of dynorphin and neurokinin B immunoreactivity in the rat hypothalamus: Morphologic evidence of interrelated function within the arcuate nucleus. J Comp Neurol 498, 712–726. [PubMed: 16917850]
74. Morin LP, Fitzgerald KM, and Zucker I (1977). Estradiol shortens the period of hamster circadian rhythms. Science 196, 305–307. [PubMed: 557840]

75. Ogawa S, Chan J, Gustafsson JA, Korach KS, and Pfaff DW (2003). Estrogen increases locomotor activity in mice through estrogen receptor alpha: Specificity for the type of activity. Endocrinology 144, 230–239. [PubMed: 12488349]
76. Driver HS, Dijk DJ, Werth E, Biedermann K, and Borbely AA (1996). Sleep and the sleep electroencephalogram across the menstrual cycle in young healthy women. J Clin Endocrinol Metab 81, 728–735. [PubMed: 8636295]
77. Smarr BL, Zucker I, and Kriegsfeld LJ (2016). Detection of Successful and Unsuccessful Pregnancies in Mice within Hours of Pairing through Frequency Analysis of High Temporal Resolution Core Body Temperature Data. PLoS One 11, e0160127. [PubMed: 27467519]
78. Mong JA, and Cusmano DM (2016). Sex differences in sleep: impact of biological sex and sex steroids. Philos Trans R Soc Lond B Biol Sci 371, 20150110. [PubMed: 26833831]
79. Hadjimarkou MM, Benham R, Schwarz JM, Holder MK, and Mong JA (2008). Estradiol suppresses rapid eye movement sleep and activation of sleep-active neurons in the ventrolateral preoptic area. Eur J Neurosci 27, 1780–1792. [PubMed: 18371078]
80. Shughrue PJ, Lane MV, and Merchenthaler I (1997). Comparative distribution of estrogen receptor-alpha and -beta mRNA in the rat central nervous system. J Comp Neurol 388, 507–525. [PubMed: 9388012]
81. Allison KC, Spaeth A, and Hopkins CM (2016). Sleep and Eating Disorders. Curr Psychiatry Rep 18, 92. [PubMed: 27553980]
82. Gore BB, Soden ME, and Zweifel LS (2013). Manipulating gene expression in projection-specific neuronal populations using combinatorial viral approaches. Curr Protoc Neurosci 4, 4 35 31–34 35 20.
83. Wang W, Darvas M, Storey GP, Bamford IJ, Gibbs JT, Palmiter RD, and Bamford NS (2013). Acetylcholine encodes long-lasting presynaptic plasticity at glutamatergic synapses in the dorsal striatum after repeated amphetamine exposure. J Neurosci 33, 10405–10426. [PubMed: 23785153]
84. Han S, Tai C, Westenbroek RE, Yu FH, Cheah CS, Potter GB, Rubenstein JL, Scheuer T, de la Iglesia HO, and Catterall WA (2012). Autistic-like behaviour in Scn1a+/− mice and rescue by enhanced GABA-mediated neurotransmission. Nature 489, 385–390. [PubMed: 22914087]
85. de la Iglesia HO (2007). In situ hybridization of suprachiasmatic nucleus slices. Methods Mol Biol 362, 513–531. [PubMed: 17417038]
86. Lee ML, Katsuyama AM, Duge LS, Sriram C, Krushelnytskyy M, Kim JJ, and de la Iglesia HO (2016). Fragmentation of Rapid Eye Movement and Nonrapid Eye Movement Sleep without Total Sleep Loss Impairs Hippocampus-Dependent Fear Memory Consolidation. Sleep 39, 2021–2031. [PubMed: 27568801]
87. Hsu YA, Gile JJ, Perez JG, Morton G, Ben-Hamo M, Turner EE, and de la Iglesia HO (2017). The Dorsal Medial Habenula Minimally Impacts Circadian Regulation of Locomotor Activity and Sleep. J Biol Rhythms 32, 444–455. [PubMed: 28954569]
88. Bronson FH, and Vom Saal FS (1979). Control of the preovulatory release of luteinizing hormone by steroids in the mouse. Endocrinology 104, 1247–1255. [PubMed: 571329]
89. Zhang C, Bosch MA, Qiu J, Ronnekleiv OK, and Kelly MJ (2015). 17beta-Estradiol increases persistent Na(+) current and excitability of AVPV/PeN Kiss1 neurons in female mice. Mol Endocrinol 29, 518–527. [PubMed: 25734516]

HIGHLIGHTS

- Kiss1^{ARH} neurons are necessary for the circadian alignment of feeding in mice
- Toxin-induced silencing of Kiss1^{ARH} neurons disrupts circadian rhythms
- Activity and sleep patterns are disrupted in the absence of Kiss1^{ARH} signaling
- Kiss1^{ARH} neurons are a component of circadian thermoregulation

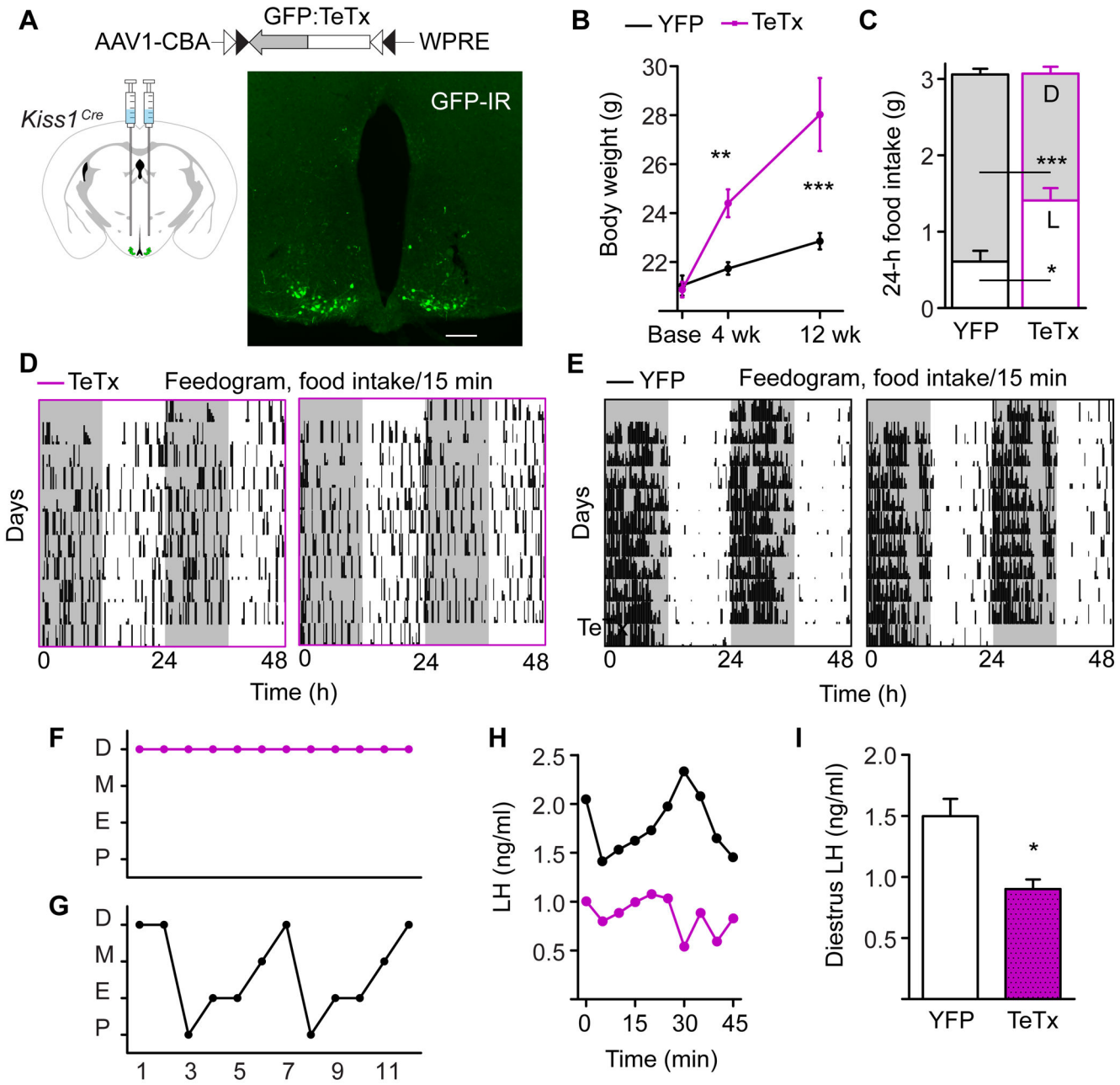

Figure 1. Kiss1^{ARH}-silenced Females are Obese, Do Not Eat More than Controls, but have Arrhythmic Feeding Patterns

A) AAV1 viral construct containing a GFP-fused TeTx transgene flanked by inverted lox sequences and driven off of the neuron-specific *Syn* promoter. The virus was injected into the ARH of *Kiss1^{Cre}* female mice. Fluorescent image of Gfp:TeTx-expressing *Kiss1^{Cre}* neurons, showing GFP immunoreactivity. Scale bar, 100 μm. Unless otherwise indicated, control mice received an inert AAV1-Ef1a-DIO-YFP reporter virus.

B) Body weight of adult female mice starting from the time of viral injection (base). Two-way ANOVA: n = 20 (TeTx at baseline, 4 wk), n = 20 (YFP at baseline, 4 wk), n = 12 (TeTx, 12 wk), n = 15 (YFP at 12 wk) , $F_{(1,99)} = 29.60$, $p < 0.0001$ (main effect of TeTx). Post-hoc,

Bonferroni comparisons at each timepoint are indicated on the graph. ** $p < 0.01$, ***$p < 0.001$.

C) Average 24-h food intake with light:dark-phase distribution. Two-way ANOVA: n = 8 (TeTx), n = 8 (YFP), $F_{(1, 108)} = 82.62$, $p < 0.0001$ (main effect of phase of consumption); $F_{(1, 108)} = 0.002$, $p = 0.97$ (main effect of TeTx on total intake); $F_{(1, 108)} = 47.82$, $p < 0.0001$ (LD x TeTx interaction).

D and E) Representative feedograms of $Kiss1^{ARH}$-silenced (D) compared to YFP-injected controls (E). Each line of the feedogram represents 48-h of double-plotted feeding patterns. Each tick is a 15-min bin, and the height of the tick indicates the amount of food consumed within a bin (bin maximum = 0.06 g).

F and G) Representative estrous cycles of TeTx (F) and YFP (G) mice. Cycling data for all of the animals in the study are shown in Figure S1B-D. Abbreviations: P, proestrus; E, estrus; M, metestrus; D, diestrus

H) Matched LH values for the representative mice shown in Figure 1F and 1G (top black line, YFP trace; bottom magenta trace, TeTx).

I) 45-min average values of LH, collected in diestrus. Student t-test: YFP n = 3, LH = 1.50 ± 0.14 ng/ml; TeTx n = 3, LH = 0.90 ± 0.08 ng/ml, $t_{(4)} = 3.67$, $p = 0.021$.

See also Figures S1 – S3.

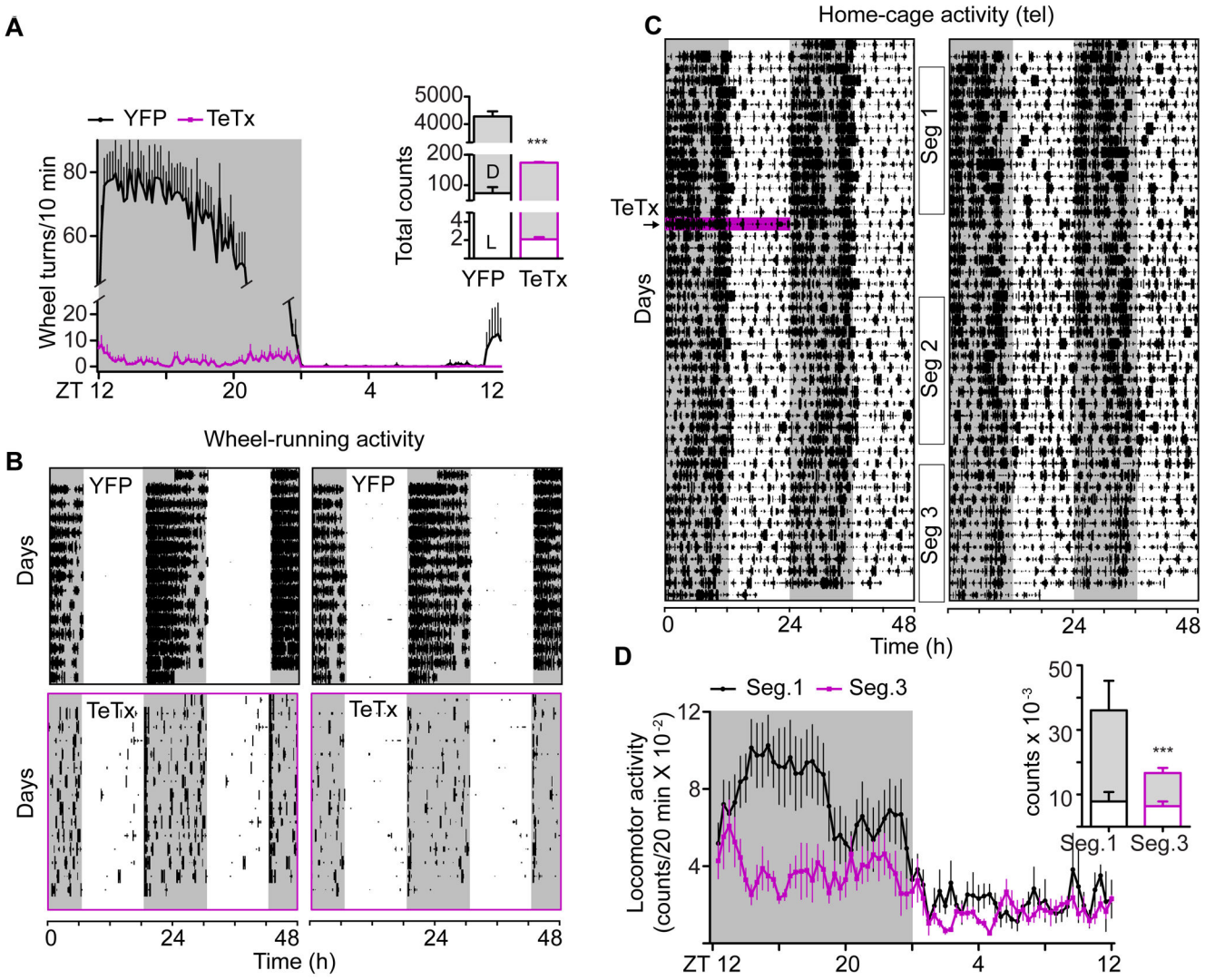

Figure 2. Kiss1^{ARH} Neuron Signaling is Necessary for Robust Dark-phase Locomotor Activity

A) Waveform of daily running-wheel activity. 3-d average for each mouse. Two-way ANOVA: n = 8 (TeTx), n = 7 (YFP), $F_{(1, 2002)} = 57.61$, $p < 0.0001$ (main effect of TeTx); $F_{(143, 2022)} = 27.55$, $p < 0.0001$ (group x time interaction). Insert shows the 24-h cumulative wheel activity in the light and dark phases of the L:D cycle. Two-way ANOVA: $F_{(1, 28)} = 465.7$, $p < 0.0001$ (main effect of TeTx).

B) Double-plotted actograms of running-wheel activity from two representative mice in each cohort. Note, the activity of Kiss1^{ARH}-silenced mice (bottom, purple boxes) was amplified by a factor of 25X in order to visualize the pattern of wheel-running activity in each 10-min bin.

C) Double-plotted actograms of home-cage activity from two representative mice, recorded with telemetry IP transponders. The pink line indicates the day of viral injection.

D) Waveform of home-cage activity counts (3 d average for each mouse) comparing the *Kiss1*^{Cre} females before (black, Seg.1) and after viral injection (purple, Seg.3). Two-way rmANOVA: n = 6, $F_{(1, 360)} = 230.7$, $p < 0.0001$ (segment effect); $F_{(71, 360)} = 3.59$, $p <$

0.0001 (segment x time interaction). Insert shows the 24-h cumulative home-cage activity in the light and dark phases of the L:D cycle. Two-way ANOVA: $F_{(1, 10)} = 21.80$, $p = 0.0009$ (main effect of TeTx).

Error bars represent ± SEM. Grey shade indicates the dark phase of the L:D cycle. See also Figures S2 and S3

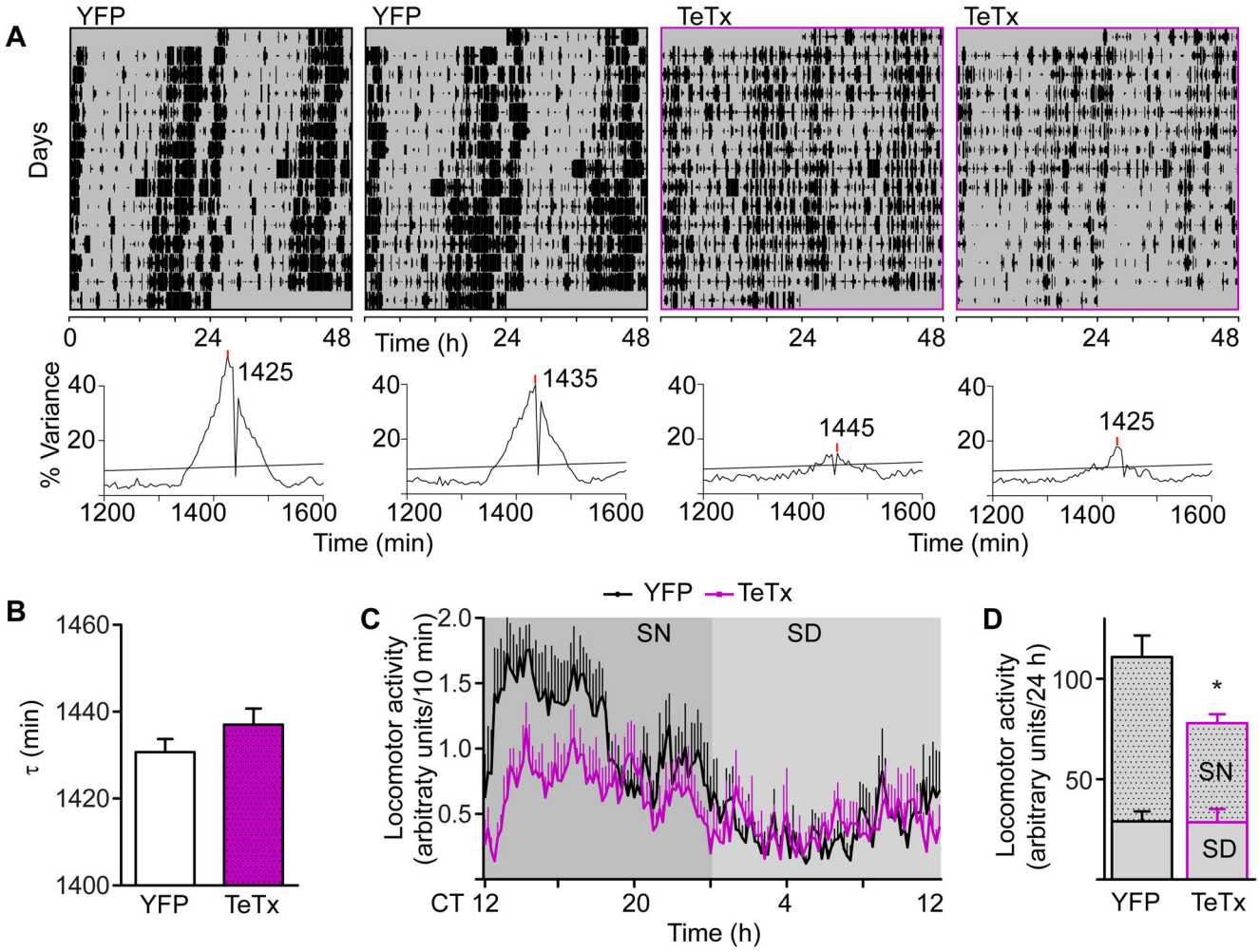

Figure 3. Circadian Home-cage Activity of Kiss1^{ARH}-silenced Mice Shows Decreased Amplitude.

A) Representative actograms of home-cage activity (tracked with infrared beams) from two mice in each cohort, double plotted. Corresponding χ^2 periodograms are shown below each actogram. Statistical significance (p = 0.05) is shown as a horizontal line.

B) Average period (t) of home-cage free-running locomotor activity comparing YFP-injected controls to Kiss1ARH-silenced females. Student t-test: YFP n = 7, t = 1431 ± 7.87 min; TeTx n = 5, t = 1437 ± 8.37 min, $t_{(10)} = 1.33$, p = 0.21.

C) Waveform of daily activity. 5-d average was calculated based on the free-running period of each mouse. CT 12:00 was aligned with the onset of activity. We assumed the subjective night to be from CT 12:00-0:00 (12 circadian hours). Two-way ANOVA: YFP (n = 7), TeTx (n = 5); $F_{(1, 1430)} = 6.36$, p = 0.03 (main effect of TeTx).

D) Cumulative 24-h activity counts, grouped into subjective day (SD) and night (SN). Student t-test comparison: YFP n = 7, t = 110.9 ± 26.45 min; TeTx n = 5, t = 77.92 ± 14.27 min, $t_{(10)} = 2.52$, p = 0.030.

See also Figure S2 and S3

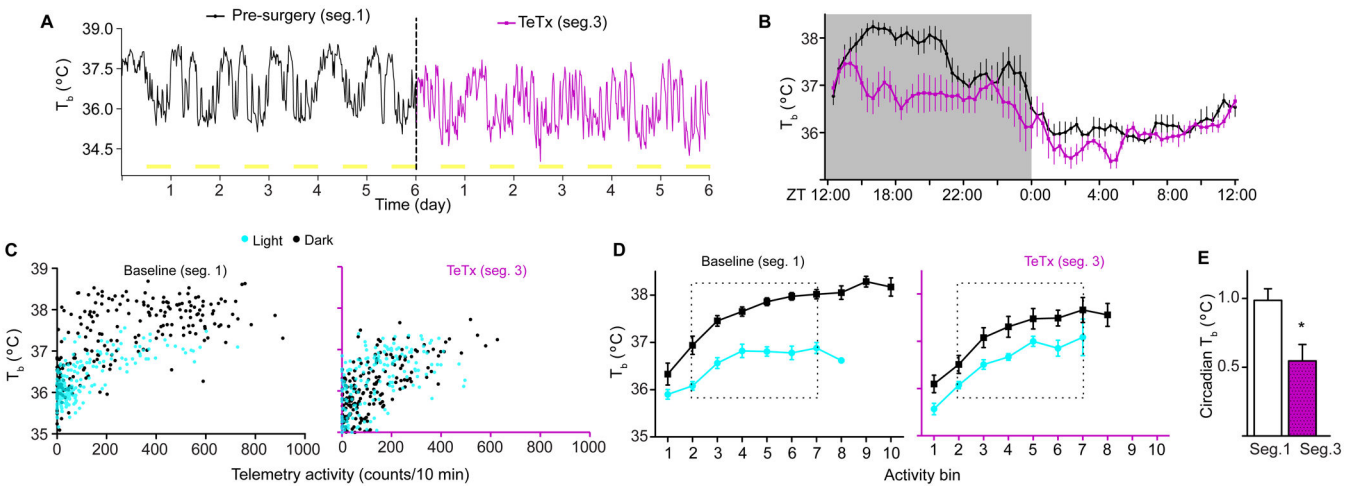

Figure 4. Kiss1^{ARH} Neurons are Necessary to Maintain the Amplitude of Core-body Temperature Rhythms Under L:D Conditions.

A) Core-body temperature (T_b) of a representative *Kiss1^{cre}* female, before and after Kiss1^{ARH} silencing (2 wk post viral injection).

B) Average amplitude of T_b before and after Kiss1^{ARH} silencing. Within subject comparison, two-way rmANOVA: n = 6, $F_{(1, 360)} = 149.4$, $p < 0.0001$. Main effect of TeTx silencing.

C) Representative mouse before (baseline/segment1) and after Kiss1^{ARH} silencing (TeTx/segment 3). Tb is plotted as a function of activity and segregated into L (turquoise dots) and D (black dots) phases. Single T_b measurements are plotted against the sum of activity 10 min prior to time of each temperature measurement.

D) Summary values of T_b vs activity for all mice in the cohort. For common point comparisons, activity counts were segregated into bins of 10 activity units, and Tb recordings within each bin were first averaged for each animal, and then the mean ± SEM was calculated for all animals.

E) Circadian T_b was calculated as the difference of mean T_b between D to L phases fore each bin (bins 2 to 7) in part **D** for each animal. The the mean ± SEM was calculated for all animals by phase. Paired-student's t-test comparison n = 6, $t_{(5)} =$, $p = 0.012$

Baseline (segment 1) and TeTx (segment 3) are defined in Figure 2. See also Figure S4

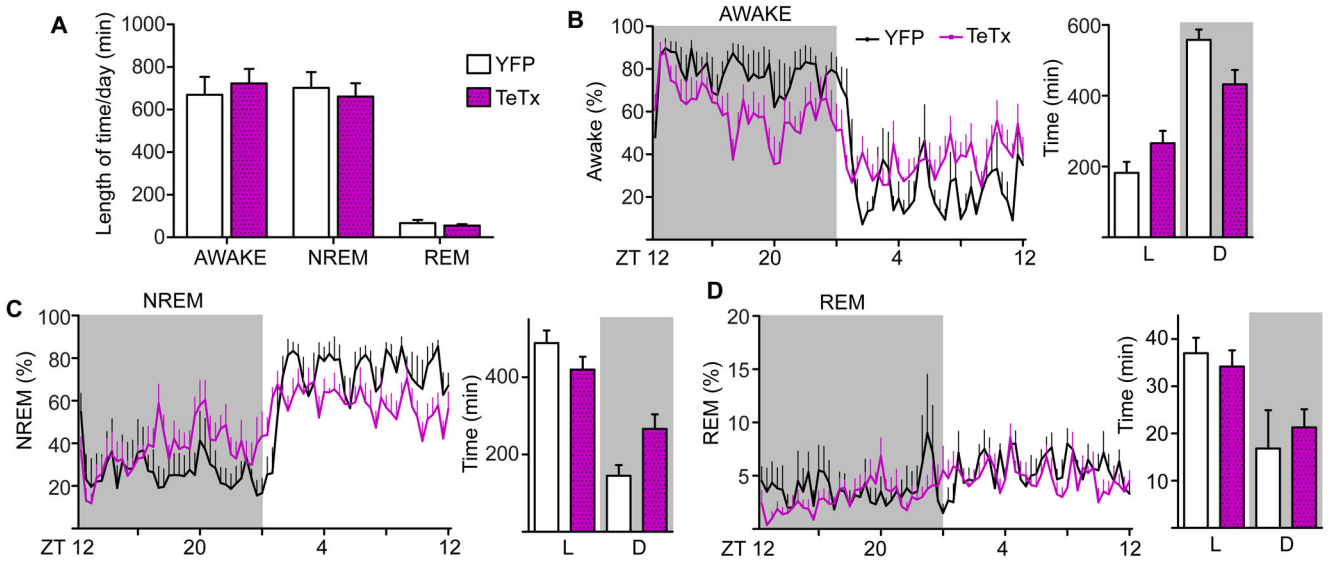

Figure 5. Sleep-wake Patterns are Influenced by Kiss1^{ARH} Neuron Transmission in L:D.

A) 24-h average of wakefulness, NREM and REM sleep states. 48 h of recording was scored and averaged for each animal. Two-way ANOVA: YFP (n = 5), TeTxLC (n = 8); $F_{(1, 36)}$ = 0.00016, p = 0.99 (main effect of TeTx silencing); $F_{(2, 36)}$ = 0.33, p = 0.72 (group x sleep state interaction).

B) Waveform of the average % time spent awake comparing Kiss1^{ARH}-silenced and YFP controls. Two-way ANOVA: YFP (n = 5), TeTx (n = 8); $F_{(71, 781)}$ = 2.89, p < 0.0001 (group x time interaction). Total wake time per phase, two-way ANOVA $F_{(1, 22)}$ = 10.37, p = 0.004; (group x LD interaction).

C) Waveform of the average % time spent in NREM comparing Kiss1^{ARH}-silenced and YFP controls. Two-way ANOVA: YFP (n = 5), TeTx (n = 8); $F_{(71, 781)}$ = 3.00, p < 0.0001 (group x time interaction). Total NREM sleep time per phase, two-way ANOVA $F_{(1, 22)}$ = 11.90, p = 0.002; (group x LD interaction).

D) Waveform of the average % time spent in REM comparing Kiss1^{ARH}-silenced and YFP controls. Two-way ANOVA: YFP (n = 5), TeTx (n = 8); $F_{(71, 781)}$ = 1.09, p = 0.288 (group x time interaction). Total NREM sleep time per phase, two-way ANOVA $F_{(1, 22)}$ = 1.51, p = 0.23; (group x LD interaction).

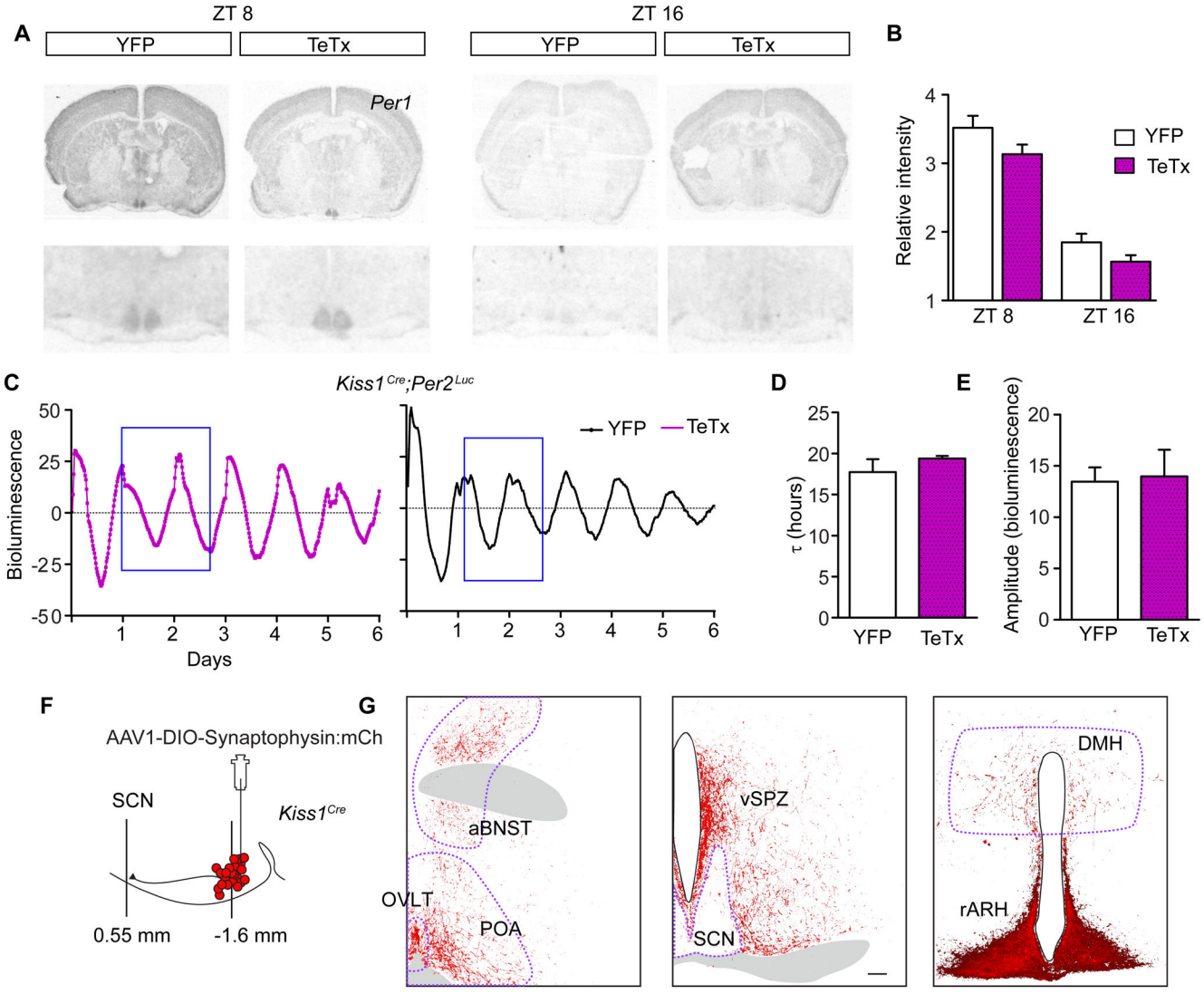

Figure 6. Kiss1^{ARH} Neurons Send Sparse Projections to the SCN and are Not Necessary for Circadian Clock Gene Expression in the SCN

A) Autoradiographic images of coronal brain sections radiolabeled with a *Per1* probe at ZT8 or ZT16.

B) Average SCN pixel intensity in autoradiographic films. One-way ANOVA: YFP (CT8 n = 8; CT16 n = 6), TeTx (CT8 n = 8; CT16 n = 4); $F(3,24) = 5.67$, $p < 0.0001$. Bonferroni post hoc comparison at CT8 and CT16. YFP was not different from TeTx at either time point.

C) Representative traces of *Per2-luc* bioluminescence rendered from time-lapsed images taken every 20 min over 6 days from control and Kiss1^{ARH}-silenced mice.

D) Average period (t) from 6 d of luminescence recordings comparing YFP-injected controls to Kiss1^{ARH}-silenced females. Student t-test, YFP n = 3, t = 17.9 ± 1.57 h; TeTx n = 3, t = 19.4 ± 0.53 h, $t_{(4)} = 1.57$, $p = 0.19$.

E) Average amplitude for 2 d of luminescence recording (blue box in E). Student t-test, YFP n = 4, amplitude = 26.91 ± 5.36 arbitrary units; TeTx n = 6, amplitude = 27.95 ± 12.68 arbitrary units, $t_{(8)} = 0.15$, $p = 0.88$.

F) Schematic diagram of the targeted viral injection of a conditional synaptophysin-fused-mCherry-reporter transgene into the ARH of *Kiss1*^{cre} females and the sagittal location of the ARH with respect to the SCN.

G) Kiss1^{ARH} fiber expression throughout the mid-rostral hypothalamus, including the SCN. Tissue was immuno-stained for the mCherry reporter (A). Scale bar, 100 mm.

Abbreviations: anterior bed nucleus of the stria terminalis, aBNST; organum vasculosum lamina terminalis, OVLT; pre optic area, POA; ventral subparaventricular zone, vSPZ; suprachiasmatic nucleus, SCN; dorsal medial hypothalamus, DMH; arcuate nucleus of the hypothalamus, ARH.

See also Figures S5 and S6